High-order vibration modes of bimetallic Ag-Au nanoparticles embedded in glass

S. Adichtchev,[1] S. Sirotkin,[1] G. Bachelier,[2] L. Saviot,[3] S. Etienne,[4] B. Stephanidis,[1] E. Duval,[1] and A. Mermet[1]

[1]*Laboratoire de Physico-Chimie des Matériaux Luminescents, Université de Lyon, UMR 5620 CNRS, Université Claude Bernard Lyon 1, 69622 Villeurbanne, France*

[2]*Laboratoire de Spectroscopie Ionique et Moléculaire, Université de Lyon, UMR 5579 CNRS, Université Claude Bernard Lyon 1, 69622 Villeurbanne, France*

[3]*Institut Carnot de Bourgogne, UMR 5209 CNRS, Université de Bourgogne, 9 av. A. Savary, BP 47870, 21078 Dijon Cedex, France*

[4]*Ecole Européenne d'Ingénieurs en Génie des Matériaux, Nancy Université, 6 rue Bastien Lepage, 54010 Nancy Cedex, France*

High-resolution low-frequency Raman scattering measurements from embedded AgAu nanoparticles unveil efficient scattering by harmonics of both the quadrupolar and the spherical modes. Comparing the experimental data with theoretical calculations that account for both the embedding medium and the resonant Raman process enables a very complete description of the observed multiple components in terms of harmonics of both the quadrupolar and spherical modes, with a dominating Raman response from the former ones. It is found that only selected harmonics of the quadrupolar mode contribute significantly to the Raman spectra in agreement with earlier theoretical predictions.

PACS number(s): 78.30.−j, 63.22.−m

Over the past 20 years, low-frequency vibrational modes from solid nanoparticles have emerged as original features of nanometer-sized matter. These modes arise from the recombination of acoustic modes that turn from *extended* to *confined* upon reducing the size of the solid. Raman scattering is a dedicated technique to probe nanoparticle oscillation modes provided that the used spectrometers are able to reach the low-frequency range where these modes typically show up ($\sigma < 10$ cm^{-1}). It has proven to be a powerful tool for a quick and nondestructive evaluation of the sizes of the nanoparticles, especially in the case of metallic ones for which Raman scattering is performed in resonance with the localized surface plasmon excitations. Under these conditions, the Raman activity of selected vibration modes of the nanoparticles is strongly enhanced so that intense signals can be obtained from very diluted nanoparticle assemblies.[1,2] Metallic nanoparticles have allowed significant progress in the understanding of nanoparticle modes such as shape anisotropy effects from Ag nanocolumns and nanolentils[3] and elastic anisotropy effects in Au nanocrystals.[2,4] Concomitantly, the theoretical description of the Raman spectra from nanoparticle vibrations has significantly improved over the years: while the free sphere model of Lamb,[5] combined with appropriate Raman selection rules,[6] initially provided satisfactory predictions of the mode frequencies,[7] coupling with the vibrations inside a surrounding matrix in the case of *embedded* nanoparticles has been well accounted for.[8,9] On the other hand, quantum calculations on *free* metal nanospheres, taking into account the vibration-plasmon coupling, have shown to be able to describe the resonant Raman spectrum in a rather complete way both in terms of frequencies and Raman intensities.[10] In particular, this latter work predicted that the Raman intensities from the quadrupolar mode harmonics are not a monotonic function of the mode index. The measurements presented in this work, which show an unusually high number of low-frequency Raman peaks, are an experimental proof of the nonmonotonic variation in intensity. Thanks to the observation of high-order harmonics, we show that the interpretation of low-frequency Raman data from metallic

nanoparticles requires taking into account not only the coupling of the surface plasmon with the different vibrations but also the influence of the surrounding matrix as well as the elastic anisotropy inside the nanoparticle.

Bimetallic AgAu nanoparticles were produced in a bulk multicomponent glass, starting from the incorporation of silver and gold salts to the initial oxide powder mix. After the colorless glass is made, prolonged annealings slightly above the glass transition temperature generate a characteristic amber shade that arises from the surface plasmon resonance (SPR) of the nucleated metallic nanoparticles. The optical characterization of four samples annealed at 490 °C over 8, 16, 32, and 64 H shows a single surface plasmon resonance peak around 445 nm (Fig. 1). This value typically lies between that of pure silver (414 nm) and that of pure gold (529 nm) when embedded as pure nanoparticles with comparable sizes in the same glass, using the same synthesis route. Upon increase of the annealing time, the AgAu SPR is redshifted,
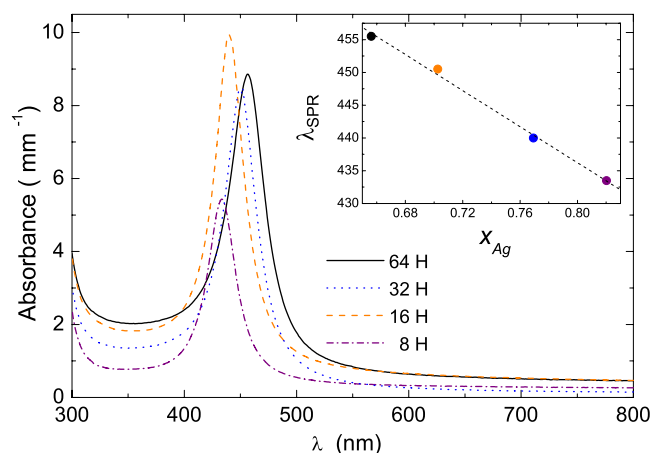

FIG. 1. (Color online) Absorption spectra of glasses containing Ag$_x$Au$_{1-x}$ nanoparticles for different annealing times. The inset shows the SPR peak position as a function of the Ag composition; the dashed line is a guide to the eyes.
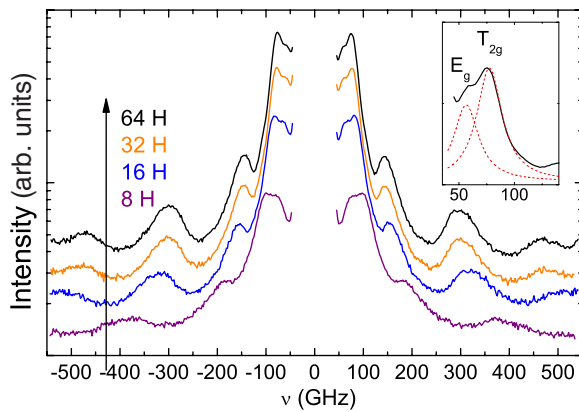
FIG. 2. (Color online) Polarized (*VV*) low-frequency Raman spectra (in log-linear scale) of AgAu nanoparticles embedded in glasses annealed over different times. Inset: enlargement of the lower (E_g, T_{2g}) doublet for the 64 H sample.

thus reflecting a gold enrichment of the bimetallic nanoparticles. Following a classical interpretation of these data,[11] one can derive the composition ratio x of the so-produced Ag_xAu_{1-x} nanoparticles as a function of annealing time t_a using a linear combination of the SPR peak positions,

$$\lambda_{Ag_xAu_{1-x}}(t_a) = x\lambda_{Ag}(t_a) + (1-x)\lambda_{Au}(t_a), \qquad (1)$$

where $\lambda_{Ag}(t_a)$ and $\lambda_{Au}(t_a)$ are, respectively, the pure Ag and the pure Au nanoparticles produced in the same glass at exactly the same annealing times. The so-derived values of x are found to decrease from 0.82 to 0.66 as the annealing times, respectively, increase from 8 to 64 H.

The low-frequency Raman scattering spectra were recorded with a six pass tandem Fabry-Perot interferometer using the 532 nm line of a continuous doubled yttrium aluminum garnet laser of 150 mW power. The scattered light was collected in backscattering geometry, and the free spectral range was set to 550 GHz. The finesse and optical contrast of such interferometer are typically greater than 100 and 10^{10}, respectively. More details on the tandem Fabry-Perot interferometer can be found elsewhere.[12,13]

As a general illustration, Fig. 2 reports the polarized spectra (with incident and scattered light polarized both vertically, *VV*) of the afore characterized samples. Quite similarly to recent observations,[2] these spectra are remarkably richer than those usually reported for metallic nanoparticles in the sense that they evidence more components than the usually two observed ones, i.e., the fundamental vibrations of both the quadrupolar mode $(\ell=2, n=1)$ and the spherical mode $(\ell=0, n=1)$ (ℓ denotes the angular momentum and n the harmonic rank). Four main bands can already be identified, some of which feature subcomponents. For purposes of illustration, we will consider in the rest of the Rapid Communication only the longest annealed sample ($Ag_{0.66}Au_{0.34}$) provided that the same analysis applies equally well to all samples.

A classical way of identifying the several components of a low-frequency Raman scattering spectrum is to compare the polarized (*VV*) and depolarized (*VH*) spectra since quadru-

polar modes and spherical modes behave differently with regards to polarization. In a first step, we focus on the *VH* spectrum which is more simple as it only features contributions from the depolarized quadrupolar modes. A multi-Lorentzian decomposition of the *VH* spectrum reveals five components, with two of them forming an intense lower-frequency doublet (Fig. 2, inset), evidenced thanks to the high-resolution Raman setup. Following recent works,[2,4] such doublet can be safely identified with the splitting of the fundamental mode of the quadrupolar vibration $(\ell=2, n=1)$ due to the high crystallinity of the nanoparticles (i.e., elastic anisotropy). Indeed, the observed frequency ratio between the lower and the larger components of the doublet, respectively, labeled as E_g and T_{2g} according to the irreducible representation of the corresponding vibrations of a face centered cubic nano*crystal*, is close to the value expected for free Au or free Ag nanocrystals[4] ($\nu_{T_{2g}}/\nu_{E_g} \simeq 1.4$ vs ~ 1.6, respectively).

As suggested by previous theoretical works,[10,14] the higher-frequency components of the depolarized Raman spectrum (approximately located at 150, 300, and 460 GHz) may be ascribed to selected high-order harmonics of the quadrupolar mode. Similar predictions have been made recently for CdS_xSe_{1-x} nanoparticles using different Raman scattering mechanisms.[15] In the following we compare our experimental results to Raman scattering intensity (RSI) calculations based on the approach developed by Bachelier and Mlayah.[10] In this approach, the low-frequency Raman spectrum of a metallic nanoparticle is generated from the calculation of the Raman transition probabilities using a three-step scattering process involving the dipolar plasmon state. For the herein investigated case, this calculation method was extended to the case of an *embedded* nanoparticle, through the determination of the continuum frequency spectrum of the nanoparticle-matrix system. A perfect contact between the particle and the matrix was assumed in order to apply the standard boundary conditions between the two media. The full derivation of the vibration modes and their normalization is out of the scope of the present Rapid Communication and will be described in detail elsewhere. In addition to the excitation wavelength, the input parameters of these calculations are the matrix acoustic parameters (density $\rho = 2.97$ g cm^{-3}; $V_L = 5020$ and $V_T = 3010$ m s^{-1} as derived from Brillouin light scattering measurements on the samples) together with those of the bimetallic nanoparticles that were assumed to be alloys and thus obeying linear relationships as a function of x.[16] Fig. 3 compares the experimental spectrum of the $Ag_{0.66}Au_{0.34}$ sample to its calculated counterpart. The overall aspect of the Raman spectrum is rather well reproduced in terms of band positions and relative intensities. For further discussion, the top scale of Fig. 3 indicates the predictions of the complex frequency method[8,9] (CFM), which enables rapid evaluation of the band positions for embedded nanoparticles yet without yielding the Raman intensities. In order to identify the filiation of the Raman bands with harmonics of the quadrupolar vibration from a single nanoparticle, Fig. 3 shows RSI spectra for the same nanoparticle but considered as *free*. In the absence of sufficiently reliable transmission electron microscopy data due to the buried nature of the nanoparticles, the mean diameter of the nanopar-
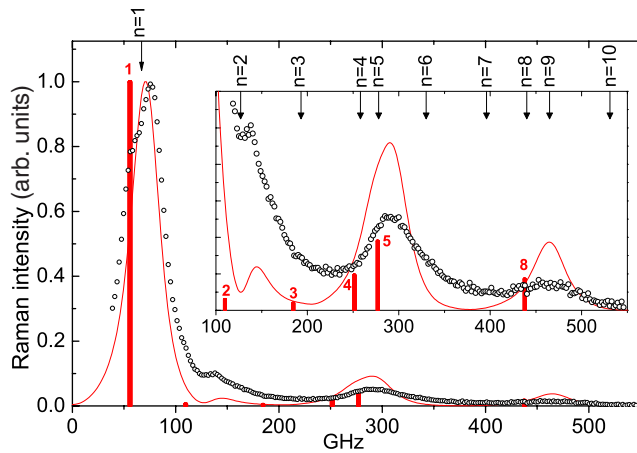
FIG. 3. (Color online) Experimental (symbols) and calculated (solid line) depolarized (VH) Raman spectra of the $Ag_{0.66}Au_{0.34}$ sample with a diameter of 23.5 nm (the spectra were normalized with respect to the ($\ell=2, n=1$) peak); high-frequency enlargement in the inset. The thick bars are the Raman intensities calculated for the same nanoparticle considered as *free*, labeled according to their n index (only harmonics with non-negligible intensities are shown). Top scale arrows: CFM predictions for the $\ell=2$ mode with the same *embedded* nanoparticle.

ticles is derived from the best fit of the lower-frequency doublet with a single average ($\ell=2, n=1$) line since at this stage the RSI calculations are unable to account for the elastic anisotropy splitting (nanocrystals are assumed as isotropic nanoparticles). The derived diameter for this system is 23.5 nm, as confirmed from the analysis of the polarized spectrum that shows in addition the spherical mode contributions.

Figure 4 compares the VV and VH experimental spectra of the $Ag_{0.66}Au_{0.34}$ sample, together with those derived from the RSI calculations. These comparisons show that the spherical mode contributions are rather small and they significantly overlap with those of the quadrupolar mode. They are better
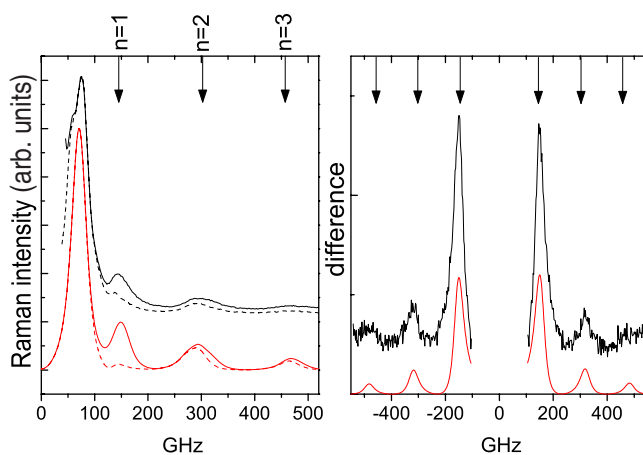

FIG. 4. (Color online) Left: experimental (upper set) and calculated (lower set) of the VV (solid) and VH (dashed) Raman profiles of the $Ag_{0.66}Au_{0.34}$ sample (intensities were normalized with respect to the ($\ell=2, n=1$) peak). Right: Raman difference spectrum ($I_{VV} - I_{VH}$), experimental (thick line) and RSI calculated (thin line). Top scales: CFM predictions for the $\ell=0$ mode.

evidenced by the Raman difference spectrum $I_{VV} - k.I_{VH}$, where k is a scaling factor chosen such that the ($\ell=2, n=1$) peaks are normalized (Fig. 4, left). The positions derived from the difference are found to well agree with the CFM predictions for the ($\ell=0, n=1, 2, 3$) modes, using the same nanoparticle size as that derived from the quadrupolar mode analysis; they are equally well consistent with the RSI predictions of band profile changes induced by the change in polarization.

The present observation of an usually rich low-frequency Raman spectrum from embedded metallic nanoparticles, and its comparison with RSI and CFM predictions, allows capture of several ingredients that are essential for a correct interpretation of similar data. The proper identification of the several Raman bands requires, in a first stage, comparison of their behavior as a function of polarization as they may result from the overlap of several contributions (Fig. 4). The detailed analysis of the depolarized spectrum, i.e., of the quadrupolar mode contributions, shows several important points. The first one is that introducing the embedding medium affects the position of the bands as displayed by the frequency mismatch of the observed bands (symbols in Fig. 3) or the CFM positions (top arrows) with the frequencies calculated in the free case (thick bars). This effect, which is essentially due to the relatively large mass density of the used glass, is most severe on the ($\ell=2, n=1$) peak, which is often used for size evaluation due to its prominence. Quantitatively, using a free case estimation based on the position of the ($\ell=2, n=1$) band leads to a 19% smaller nanoparticle diameter. The second result is that from the frequency position matching between the experimental curve and the calculated RSI and CFM contributions, it comes out that the high-frequency components are affiliated with selected harmonics, or at least harmonic groups, of the single nanoparticle vibration: the bands near 290 and 460 GHz clearly identify with, respectively, the $n=4, 5$ and $n=8$ harmonic components of the quadrupolar mode. Their respective Raman cross sections are relatively consistent with those predicted in the free sphere case (delta functions in Fig. 3).[10] The situation is somewhat less clear-cut with the weak band at 150 Ghz which well identifies with the $n=2$ harmonic in terms of frequency while its intensity is considerably stronger than that expected from the free sphere evaluation: according to RSI calculations, it is enhanced by a factor of 4 going from the free case to the embedded case while the other harmonics are enhanced by a factor of 2 (its stronger intensity in the experimental spectrum is certainly due to its merging with the foot of the T_{2g} component that the RSI calculations are unable to account for at the present stage). This enhancement is rooted in the coupling with the matrix that significantly increases the displacement at the surface of the nanoparticle, for this particular harmonic, making it a potential good probe of the coupling interface. Another possible interpretation is that the 150 GHz band results from the redistribution of mode frequencies that arises from the anistropy effect, as is observed from the splitting of the ($\ell=2, n=1$) component. These two interpretations differ from that given for a similar band observed from similar Au-doped glasses.[2]

Finally, the comparison of the RSI and CFM calculations with the experimental data provides a further interesting as-

pect related to the specificity of *resonant* Raman scattering for metallic nanoparticles. Indeed, one observes that while the frequency positions of the spherical mode bands agree well with those predicted by either RSI or CFM calculation (Fig. 4), the CFM predictions for the quadrupolar mode harmonics are systematically slightly redshifted with respect to either the experimental or the RSI calculated bands (Fig. 3). This is due to the dual nature of the quadrupolar modes (longitudinal vs transverse as defined in Ref. 14) which is also present inside a given CFM resonance. The plasmon-vibration coupling is therefore significant only for a subset of modes inside the frequency range defined by a CFM peak which can lead to a shift in the observed maxima. This situation does not occur for the spherical mode. As a result, the CFM and RSI peak positions match and these modes can be more reliably used for the size evaluation of the nanoparticles provided that they are safely extracted from the dominating quadrupolar mode response.

The first observation of high-order quadrupolar and spherical harmonic modes from AgAu nanoparticles embedded in a glass has allowed us to rationalize the interpretation of low-frequency Raman spectra from metallic nanoparticles. In accord with theoretical predictions, one observes that Raman scattering by the quadrupolar modes is not a monotonic decreasing function of the harmonic index so that only selected harmonics participate to the Raman spectrum with differing efficiencies. Due to stronger coupling with the plasmon excitations, the Raman spectrum is strongly dominated by high-order harmonics of the quadrupolar modes that overlap with the weaker polarized signatures from the spherical modes. In such case, a detailed polarization analysis of the Raman bands is therefore essential to check the band assignments that are uniquely based on frequency position matchings.[17,18]

---

[1] A. Courty, I. Lisiecki, and M. P. Pileni, J. Chem. Phys. **116**, 8074 (2002).

[2] B. Stephanidis, S. Adichtchev, S. Etienne, S. Migot, E. Duval, and A. Mermet, Phys. Rev. B **76**, 121404(R) (2007).

[3] J. Margueritat, J. Gonzalo, C. Afonso, G. Bachelier, A. Mlayah, A. Laarakker, D. Murray, and L. Saviot, App. Phys. A **89**, 369 (2007).

[4] H. Portalès, N. Goubet, L. Saviot, S. Adichtchev, D. B. Murray, A. Mermet, E. Duval, and M.-P. Pileni, Proc. Natl. Acad. Sci. U.S.A. **105**, 14784 (2008).

[5] H. Lamb, Proc. London Math. Soc. **s1-13**, 189 (1881).

[6] E. Duval, Phys. Rev. B **46**, 5795 (1992).

[7] E. Duval, A. Boukenter, and B. Champagnon, Phys. Rev. Lett. **56**, 2052 (1986).

[8] V. Dubrovskiy and V. Morochnik, Izv., Acad. Sci., USSR, Phys. Solid Earth **17**, 494 (1981).

[9] P. Verma, W. Cordts, G. Irmer, and J. Monecke, Phys. Rev. B **60**, 5778 (1999).

[10] G. Bachelier and A. Mlayah, Phys. Rev. B **69**, 205408 (2004).

[11] S. Link, Z. Wang, and M. El-Sayed, J. Phys. Chem. B **103**, 3529 (1999).

[12] J. R. Sandercock, *Trends in Brillouin Scattering: Studies of Opaque Materials, Supported Films, and Central Modes* (Springer-Verlag, Berlin, 1982), Chap. 6, pp. 173–206.

[13] R. Mock, B. Hillebrands, and R. Sandercock, J. Phys. E **20**, 656 (1987).

[14] L. Saviot and D. B. Murray, Phys. Rev. B **72**, 205433 (2005).

[15] D. Ristić, M. Ivanda, K. Furić, U. V. Desnica, M. Buljan, M. Montagna, M. Ferrari, A. Chiasera, and Y. Jestin, J. Appl. Phys. **104**, 073519 (2008).

[16] Alloy properties P^a ($P = \rho, V_L, V_T$) were evaluated through $P^a = x \cdot P^{Ag} + (1-x) \cdot P^{Au}$, using $\rho^{Ag} = 10.5$ g cm^{-3}, $\rho^{Au} = 19.28$ g cm^{-3}, $V_L^{Ag} = 3747$ m/s, $V_L^{Au} = 3319$ m/s, $V_T^{Ag} = 1740$ m/s, $V_L^{Au} = 1236$ m/s.

[17] H. Portalès, L. Saviot, E. Duval, M. Fujii, S. Hayashi, N. Del Fatti, and F. Vallée, J. Chem. Phys. **115**, 3444 (2001).

[18] A. Nelet, A. Crut, A. Arbouet, N. Del Fatti, F. Vallée, H. Portalès, L. Saviot, and E. Duval, Appl. Surf. Sci. **226**, 209 (2004).